Journal of Applied Polymer Science

Ordered mesoporous carbon preparation by the *in situ* radical polymerization of acrylamide and its application for resorcinol removal

Wan Shou,[1]* Bing Chao,[2] Zaki Uddin Ahmad,[2] Daniel Dianchen Gang[2]

[1]Department of Mechanical Engineering, University of Louisiana at Lafayette, Lafayette, Louisiana 70504

[2]Department of Civil Engineering, University of Louisiana at Lafayette, Lafayette, Louisiana 70504

*Present address: Department of Mechanical and Aerospace Engineering, Missouri University of Science and Technology, Rolla, Missouri 65409

Correspondence to: D. D. Gang (E-mail: gang@louisiana.edu)

ABSTRACT: In this study, acrylamide (AM) was, for the first time, successfully used to synthesize ordered mesoporous carbon (OMC) through *in situ* polymerization inside SBA-15 (Santa Barbara Amorphous type material) as a hard template. A straightforward and environmentally friendly method was proposed and verified with an emphasis on the precursor modification for the preparation of OMC. The influences of the structure and the amount of SBA-15 on the OMC structure and adsorption capacity were evaluated. To improve the adsorption capacity and yield, the following three approaches were tried: (1) the use of concentrated sulfuric acid (H_2SO_4) to fix carbon and nitrogen, (2) the use of a crosslinking agent, and (3) the addition of melamine as a possible nitrogen source. The adsorption capacities for resorcinol were evaluated, and they showed an improvement of 37% in comparison with that of the commercially available granular activated carbon (27 mg/g). Well-OMC materials were obtained with higher yields with H_2SO_4 and crosslinking agent compared with those obtained for the pure AM precursor. © 2016 Wiley Periodicals, Inc. J. Appl. Polym. Sci. **2016**, *133*, 43426.

KEYWORDS: adsorption; crosslinking; porous materials; properties and characterization; separation techniques

Received 28 June 2015; accepted 10 January 2016

DOI: 10.1002/app.43426

INTRODUCTION

Ordered mesoporous carbon (OMC) materials have attracted broad and growing attention because of their wide applications in catalyst supports,[1,2] electrode materials,[3] and adsorbents.[4] OMC has been thought of as an excellent adsorbent for organic pollutant removal because of its remarkable properties, such as its uniform tunable mesopores (typically in the range 2–10 nm), high specific surface areas (SSAs; up to 1800 m^2/g), and higher hydrothermal resistance compared with mesoporous silica materials and other materials.[5–7]

There are two main routes for synthesizing OMCs[8]: one is soft-template synthesis, in which block copolymers are directly self-assembled as templates for the generation of the porous carbon structure, and then OMCs are obtained through cocondensation and carbonization. The other route is hard-template synthesis, in which mesoporous silica is presynthesized as a mold and then filled with carbon precursor; this is followed by carbonization and subsequent template removal with sodium hydroxide or hydrofluoric acid (HF). Soft-template synthesis overcomes several limitations of hard-template synthesis; these include the elimination of the presynthesis of the mesoporous silica template and template removal. However, because of the strict requirements,[8] a limited number of materials[8–12] can meet these requirements. Additional disadvantages include its (1) complex and subtle multistep processes, (2) low self-assembly rate,[9,10] (3) toxicity to the operators,[9] and (4) less ordered OMC product.[12] Therefore, the hard-template approach is preferred for wider applications, and it was used in this study.

Since the first synthesis of OMC with sucrose as a carbon precursor,[13] various carbon precursors have been explored; these include poly(acrylic acid),[14] polypyrrole,[15] polyacrylonitrile,[16] and resorcinol–formaldehyde resin.[17] Acrylamide (AM) is an easily accessible and relatively cheap chemical compound. Because of its carbon–carbon double bond, amide group, and wide range of chemical reactions, it is apt to be modified during the polymerization process.

Phenolic compounds are toxic and hazardous to aquatic life and human beings,[5,18,19] even at a very low concentration (0.1 $\mu g/L$).[20] Thus, it is imperative to remove phenolic compounds from wastewater before discharging. Among all of the methods

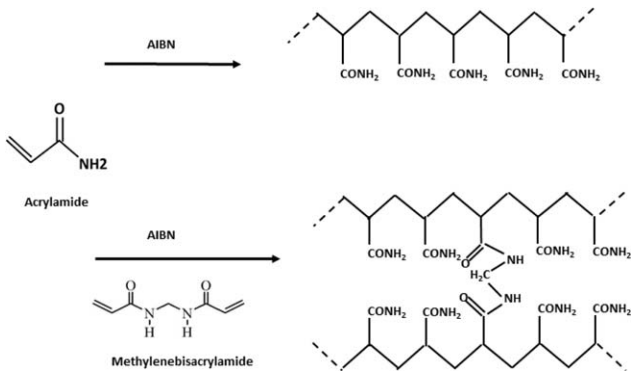

Figure 1. AM polymerization reaction.

for phenols and the removal of their derivative, such as oxidation, biodegradation, membrane separation, precipitation, extraction, and adsorption,[18,19,21–23] adsorption is considered to be the most effective method because of its sludge-free clean operation and acceptable price and the availability of various adsorbents. Activated carbons are often used for phenolic compound removal[18,19,24] because of their good performance. Generally, activated carbon-based adsorbents are composed of a large fraction of micropores (<2 nm); this can result in slow diffusion kinetics. In contrast, because the ordered mesopores possess fast adsorption kinetics and a high adsorption capacity, OMC can be used as a substitute for activated carbon in water purification.

The main characteristics of an adsorbent, such as its pore structure, functional groups, and polarity, determine the adsorption capacity. Numerous studies have been conducted to create geometrical and chemical heterogeneity in adsorbents.[5,14,21,24–26] Generally, heteroatoms contained in functional groups can be indirectly induced into OMCs through posttreatment with functionalizing agents or coated with OMC as a composite or directly incorporated into the precursor as a carbon source. To improve the adsorption capacity of OMC, Anbia and Ghaffari[25] investigated the effect of various parameters (adsorbent dose, pH, initial concentration, and contact time) on the adsorption performance of modified OMC, which was fabricated through the coating of CMK-1 with a polyaniline polymer. He *et al.*[26] prepared modified CMK-3 through chemical oxidation by ammonium persulfate and sulfuric acid (H_2SO_4) and further grafted it with 1-octanol with an esterification reaction to enhance its adsorption performance. Guo *et al.*[14] tried to impart OMC with new oxygen groups through oxidation with concentrated nitric acid. All of these methods showed considerable adsorption improvements; however, because of the relatively low reactivity of the carbon surface, posttreatment complicates the process and also increases the cost. Meanwhile, posttreatment accompanied with the use of nitric acid or other chemicals[14,27,28] may generate secondary pollution during adsorbent preparation. In addition, postmodification can result in low bonding densities and may damage the carbon surface or mesostructure;[14,24–28] for example, it can shrink the mesopore size, decrease the surface area and pore volume, and cause pore blockage. Ideally, when such functional groups can be incorporated in the carbon precursor and retained after carbonization, the desired OMC manufacturing process will become more straightforward and environmentally friendly.

Although H_2SO_4 was used as a catalyst for OMC fabrication,[13] no report has discussed its role in assisting in the retention of carbon materials during the carbonization process, and its ability to activate carbon materials has not been reported. Namely, the carbon fixation ability and activation effect[29] of H_2SO_4, where a dehydration and mild carbonization process occur, has not been considered. Crosslinking is indispensable for OMC fabrication through a self-assembly method,[8] but a crosslinking agent has not been investigated in the hard-template synthesis method. In this study, AM was, for the first time, successfully used to synthesize OMC through *in situ* radical polymerization with SBA-15 as a hard template. During the initiation reaction, 2,2′-azobisisobutyronitrile (AIBN) decomposed; this eliminated a molecule of nitrogen gas to form two 2-cyanoprop-2-yl radicals. These radicals initiated the polymerization for AM (as illustrated in the top of Figure 1). Three batches of SBA-15 (−1, −2, and −3) with different mesopore sizes were prepared through the tuning of the reaction time and temperature.[30] Then, these templates were used to investigate their influence on the properties of the fabricated OMCs. Three different approaches were used to attempt to modify the OMC: (1) the use of concentrated H_2SO_4, (2) the addition of crosslinking agent, and (3) the addition of melamine as a possible nitrogen source.

EXPERIMENTAL

Synthesis of the Silica Template

The synthesis of SBA-15 was modified from the literature.[14] Typically, 100 mL of concentrated hydrochloric acid (HCl, 37%) was added to 525 mL of distilled water to provide an acidic solution, and then, 20 g of the triblock copolymer Pluronic P123 ($EO_{20}PO_{70}EO_{20}$; BASF) was added as a surfactant to direct the formation of a mesoporous structure. Subsequently, 46.5 mL of tetraethylorthosilicate (98%, Aldrich) was added after the complete dissolution of P123. Then, the resulting mixture was vigorously stirred to form a homogeneous solution. After the reaction was completed under certain conditions (40 °C for 4 h for SBA-15-1, 50 °C for 6 h for SBA-15-2, and 60 °C for 8 h for SBA-15-3),[30] the milky white suspension was aged in a 90 °C water bath for 24 h. Then, the solid product was filtered and washed with 2000 mL of 80–90 °C distilled water and dried in an oven at 105 °C overnight. After drying, the product was calcined in an air-flow furnace at 550 °C for 8 h.

Fabrication of the OMCs

The synthesis of the OMCs was accomplished by the *in situ* polymerization of AM (≥99%, Aldrich) in a silica mesoporous template. The typical procedure is illustrated in Figure 2, where *X* and *Y* indicate the amount and batch, respectively, of the template used for synthesis. The complete abbreviations for the different OMCs are listed in Table I.

In the modification part, OMC-1 was obtained with the previous procedure of preparing OMC-22, except the distilled water was replaced by a mixture consisting of 10 mL of concentrated H_2SO_4 (96.1%, HACH) and 10 mL of distilled water. OMC-2

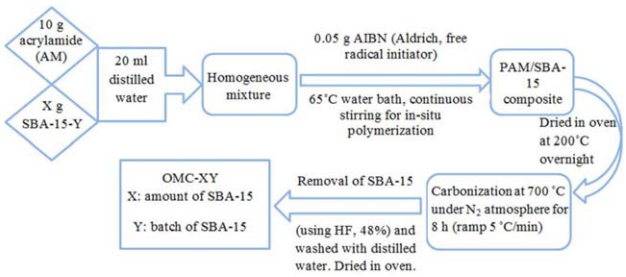

Figure 2. Flow chart of OMC fabrication. [Color figure can be viewed in the online issue, which is available at wileyonlinelibrary.com.]

was fabricated according to the flow chart for OMC-22 by the addition of an extra 0.2 g of crosslinking agent (*N,N′*-methylene bisacrylamide, Acros Organics) during the polymerization process. The effect of the crosslinking agent on polymerization is illustrated in Figure 1. OMC-3 was obtained according to the flow chart with the replacement of the distilled water with a mixture of 10 mL of concentrated H_2SO_4 and 10 mL of distilled water and the addition of an extra 0.2 g of crosslinking agent during the polymerization process. On the basis of the procedure for fabricating OMC-1, OMC-4 was obtained through the mixture of 2 g of melamine (Acros Organic) with AM and SBA-15 in an aqueous solution.

Characterization

Small-angle powder X-ray diffraction (SAXRD) patterns were recorded with a Diano 2100E powder X-ray diffractometer with Cu Kα_{12} radiation ($k = 1.5418$Å, 45 kV, 30 mA) to analyze the ordering of the mesostructure of the SBA-15 and OMCs. Transmission electron microscopy (TEM) was used to characterize the mesoporous structure of the SBA-15 and OMCs with an acceleration voltage of 80 kV with a Hitachi 7600. SBA-15 was also observed under a JEOL 6300 scanning electron microscope. The SSAs and pore textural properties were measured with a Micromeritics FlowSorb III surface area analyzer and ASAP 2020 (Accelerated Surface Area and Porosimetry System). Functional groups and chemical bonds were analyzed by Fourier transform infrared (FTIR) spectroscopy and Raman spectroscopy with a PerkinElmer Spectrum 100 FTIR spectrometer and a StellarNet's Raman laser, respectively. Main elemental components were analyzed in an Elementar Vario MICRO Cube CHNS elemental analyzer.

Adsorption Study

To evaluate the adsorption capacities of the OMCs on resorcinol, batch adsorption experiments were conducted as follows: 100 mL of resorcinol solution with a concentration of 5 mg/L (pH 6.1) was placed in both experimental (with adsorbent and

Table I. Relationship between the Templates and OMC Abbreviations

	Amount of template (g)		
Template	1	2	3
SBA-15-1	OMC-11	OMC-21	OMC-31
SBA-15-2	OMC-12	OMC-22	OMC-32
SBA-15-3	OMC-13	OMC-23	OMC-33

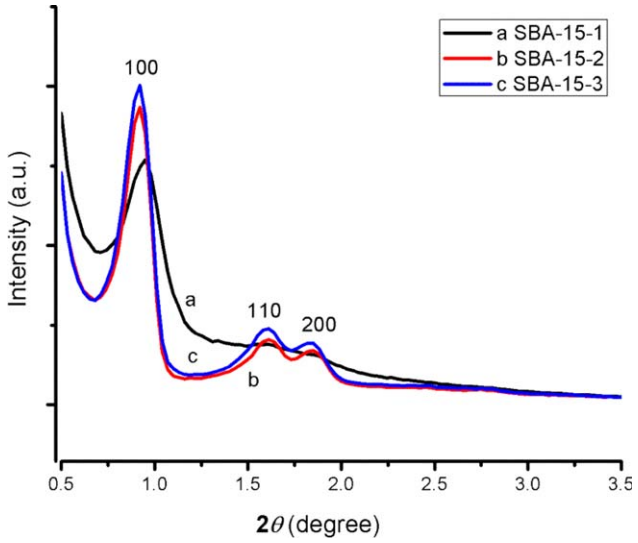

Figure 3. SAXRD patterns of different batches of SBA-15. [Color figure can be viewed in the online issue, which is available at wileyonlinelibrary.com.]

OMCs) and control (without adsorbent and regarded as blank) conical flasks. All of the samples were placed in an E 24 incubator shaker (New Brunswick Scientific) at 200 rpm at room temperature (25 °C). After 24 h, the conical flasks were removed, and the solutions were filtered with 0.45-μm glass filter paper. The blank was used as a reference to establish the initial concentration for the solutions containing OMCs. A filtered solution from the experimental flask was analyzed for the final concentration of resorcinol. The adsorption capacities of the OMCs were measured by a Cary 50 ultraviolet–visible spectrophotometer (Varian) with a wavelength of 500 nm at room temperature. The amount of resorcinol adsorbed by the OMCs was determined by the subtraction of the final concentration from the initial concentration with the following formula:

$$q = \frac{(C_i - C_f)V}{M}$$

where q is the adsorption capacity (mg/g), C_i is the initial concentration of resorcinol in the solution (mg/L), C_f is the final concentration of resorcinol in the treated solution (mg/L), V is the volume of the solution taken (L), and M is the weight of the adsorbent OMCs (g).

RESULTS AND DISCUSSION

X-ray Diffraction (XRD) Pattern of SBA-15

As depicted in Figure 3, the SAXRD patterns of different batches of SBA-15 showed well-resolved diffraction peaks indexed as (100), (110), and (200); this suggested a long-range, highly ordered, two-dimensional hexagonal mesostructure.[3,7] SBA-15-2 and SBA-15-3 had a similar trend of peaks, but SBA-15-3 had a stronger peak of (100) reflection. In a comparison of SBA-15-1 with SBA-15-2 and SBA-15-3, we noticed that when the reaction temperature was increased and the reaction time was extended, the diffraction peaks shifted to a smaller angle value with increasing intensity. Correspondingly, the *d*-spacing between (100) planes increased from 9.31 nm (SBA-15-1) to 9.60 and 9.62 nm

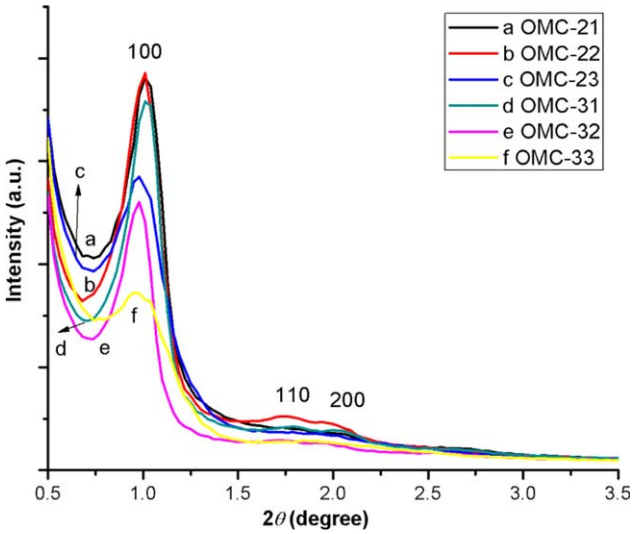

Figure 4. SAXRD patterns of OMCs prepared from different batches and different amounts of SBA-15. [Color figure can be viewed in the online issue, which is available at wileyonlinelibrary.com.]

for SBA-15-2 and SBA-15-3, respectively. We concluded that the reaction conditions played an important role in the mesostructure of the synthesized SBA-15.[30]

XRD Patterns of the OMCs

Figure 4 compares the SAXRD patterns of the OMCs with different SBA-15 templates and amounts. Here, the use of 1 g of SBA-15 was not successful for fabricating OMC; thus, no SAXRD pattern of OMC-1Y is presented. All of the carbon products had similar pattern to those of the silica templates with (100), (110), and (200) diffractions; this demonstrated the characteristics of the hexagonal structures. Well-resolved (110) and (200) peaks were observed in the OMC-22 curve, whereas weak peaks were detected for other OMCs. Compared with the SAXRD patterns of SBA-15, these weaker peaks may have resulted from the shrinkage of the composite during carbonization and the removal of the silica template.[2,15] The OMCs duplicated from SBA-15-1 (OMC-21 and OMC-31) had the highest average intensity and the ones duplicated from SBA-15-3 (OMC-23 and OMC-33) had the lowest intensity at the (100) peak. This difference was attributed to the serious shrinkage and collapse of SBA-15-3 when the reaction temperature and time increased, and it resulted in a larger pore size and thinner silica walls.[30] The interplanar distances (d_{100}'s) for OMC-21, OMC-22, and OMC-23 were 8.50, 8.75, and 9.00 nm, respectively. Similarly, the d_{100} values for OMC-31, OMC-32, and OMC-33 are 8.70, 9.00, and 9.28 nm. It is worth noting that d_{100} of the OMCs increased with the increase of their silica templates' d_{100}. We also noticed that an increase in the amount of SBA-15 caused an increase in d_{100} of the OMCs; this meant that the morphology and textural parameters of the OMCs could be adjusted through changes in the ratio of the template to the carbon precursor;[31,32] nonetheless, the intensities of the (100) peak of the corresponding OMCs decreased slightly. These changes may have resulted from the excess amount of template and may have led to the incomplete filling of the template channels.

As the modified OMCs were synthesized with 2 g of SBA-15-2, the SAXRD pattern of OMC-22 was adopted to compare the OMCs before and after modification; this is presented in Figure 5. Figure 5 shows an obvious drop in the peak intensity at the (100) peak reflection, and the (110) and (200) peaks were not as well resolved as that of their silica templates (OMC-21 and OMC-22). In other words, an ordered, two-dimensional hexagonal structure was detected, but the structure may not have been as good as those of their templates and the original OMC. These changes could have resulted from acid-catalyst effects[33] or crosslinking swelling effects,[34] which may have caused the collapse of the template walls. Another possible reason could have been the complex physicochemical reactions of H_2SO_4,[33] such as swelling and dehydration, which led to possible damage of the original structure.

Morphology of SBA-15

The microstructure of SBA-15-2 is shown in Figure 6 as a typical template; it had a regular rodlike shape with an average diameter around 0.5 μm and a length around 0.8–1 μm, similar to those in previous reports.[7] The difference in length may have resulted from the reaction temperature and time, which were believed to determine the rod length and mesopore size.[35] To further show the mesostructure of SBA-15, TEM images are exhibited in Figure 7, together with the change in the channel diameter corresponding to the reaction conditions (time and temperature). It is worth noting that increases in the reaction temperature and reaction time could increase the average channel diameter from 3 to 9 nm; this was consistent with the increasing trend of d_{100} for SBA-15, and it also agreed with the literature.[30] All of the diameters were measured by ImageJ software, with standard deviations of about 0.5 nm. The TEM images shown in Figure 7(a–c) display the parallel mesopores of SBA-15 from the (110) direction and show uniform parallel channels. The periodic hexagonal structure viewed along the (100) direction is shown in Figure 7(d) and was consistent with the SAXRD pattern. These highly ordered mesoporous structures were similar to those reported in the literature.[2,3,7,14]

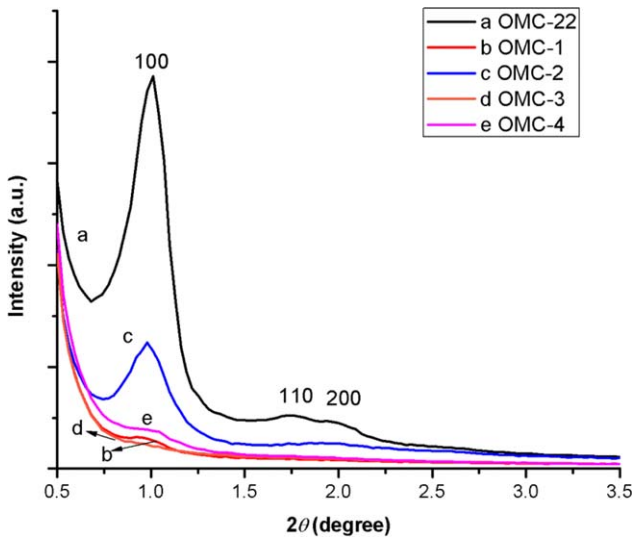

Figure 5. SAXRD pattern comparison of OMCs before and after modification. [Color figure can be viewed in the online issue, which is available at wileyonlinelibrary.com.]

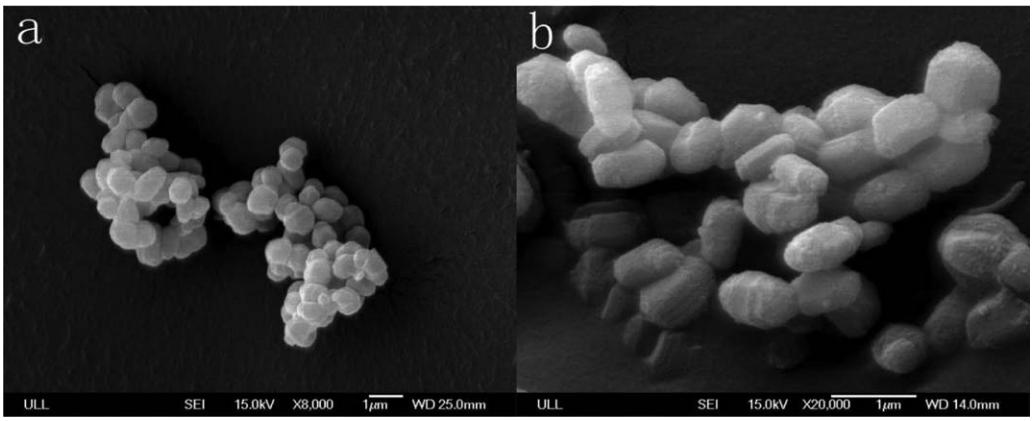

Figure 6. Scanning electron microscopy images of SBA-15-2 under different magnifications: (a) 8000 and (b) 20,000×.

TEM Characterization of the OMCs

The corresponding OMC replicas of the silica templates are illustrated in Figure 8. All of the mesostructures, with parallel ordered channels, were analogous to their templates. However, the channel diameters were smaller than their templates (ca. 0.5–1 nm); this probably resulted from the shrinkage of carbon/silica composite material during carbonization and the removal of host silica.[2,15,32] The hexagonal structure of OMC viewed from the (100) direction is shown in Figure 8(d); this is a replica of the SBA-15 structure, similar to those found in previous reports.[2,14]

We found that additions of 2 and 3 g of SBA-15 resulted in the same mesoporous structure; this further demonstrated that the mesoporous structure of OMC was a replica of the pore structure of its silica template. However, it was very interesting that the use of 1 g of SBA-15 resulted in a totally different structure of carbon materials. In this case, we failed to obtain OMC, but some hollow nanofiber-like carbons were observed.[7,32,36] This phenomenon revealed that the ratio between SBA-15 and AM played an important role in the successful replication of the ordered carbon material. Only when the amount of template was sufficient could the ordered be formed. Once the amount of template was sufficient for OMC synthesis, the structure of OMC mainly depended on the SBA-15 template structure. In the following study, the investigations were focused on the OMC-2Y and OMC-3Y series.

On the basis of the well-preserved, ordered mesoporous structure and reasonable ratio, modifications were conducted on the basis of the OMC-22 synthesis procedures. TEM images of all of the modified OMCs are depicted in Figure 9. In a comparison of the TEM images of OMCs fabricated with concentrated H_2SO_4 [Figure 9(a,c,d)] with OMC-22 [Figure 8(b)], we observed that the channels were ragged, and the mesostructure became disordered, although the main morphology was preserved, similar to that in nitric acid oxidized OMCs.[27,28] Meanwhile, the inserted perpendicular view of the hexagonal structure became more difficult to observe in these H_2SO_4-modified OMCs, and the surfaces became blurry in comparison with those of OMC-22 and previous reports.[2,14,15] In OMC-1 [Figure 9(a)], which only used H_2SO_4, such structures were not found. However, the OMC fabricated with crosslinking agent (OMC-2) maintained as well an ordered structure as OMC-22;

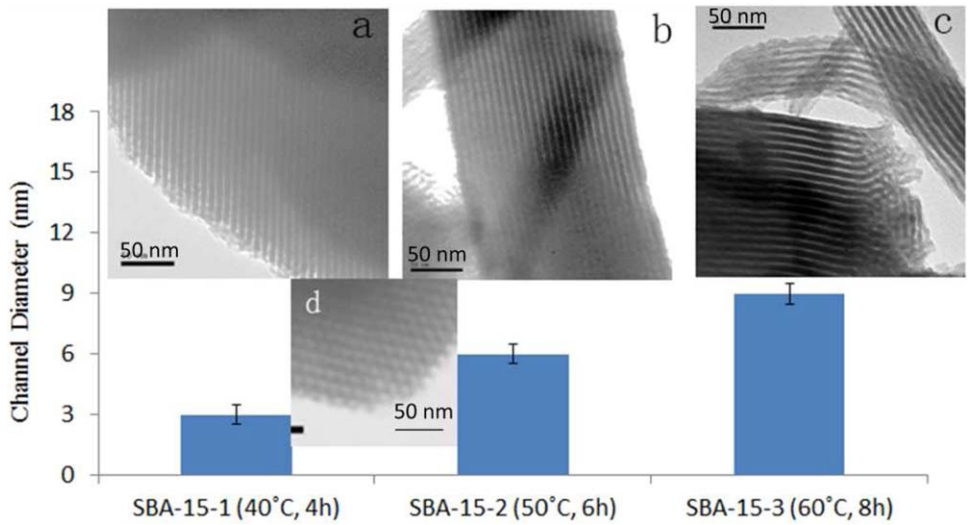

Figure 7. Influence of the reaction conditions on the SBA-15 channel diameter: (a–c) channel direction view of corresponding SBA-15 and (d) perpendicular view of SBA-15-2. [Color figure can be viewed in the online issue, which is available at wileyonlinelibrary.com.]

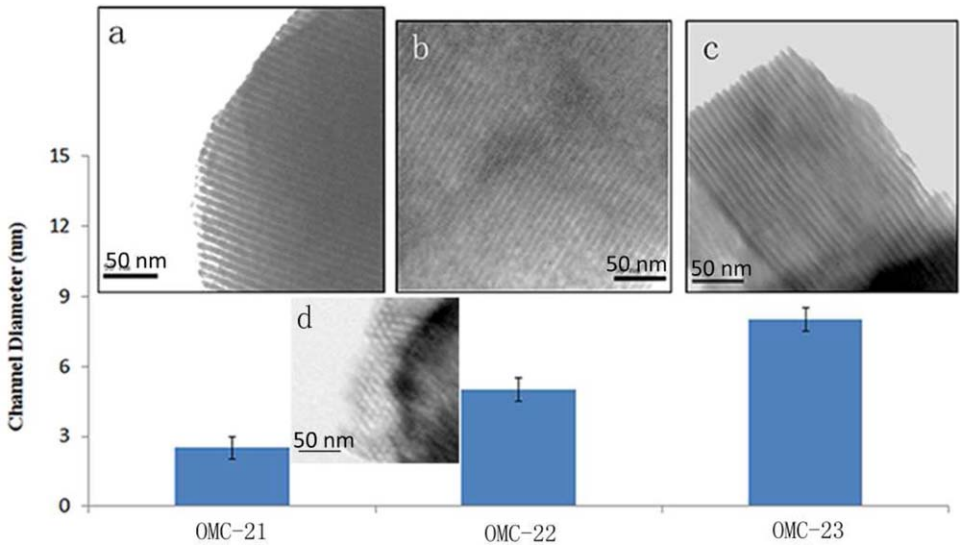

Figure 8. Influence of the different SBA-15 templates on the OMC channel diameter: (a–c) channel direction view of OMCs and (d) perpendicular view of OMC-22. [Color figure can be viewed in the online issue, which is available at wileyonlinelibrary.com.]

this was also confirmed by the SAXRD pattern in Figure 5. This surface change in OMC may have been due to the complicated physicochemical effects, such as dehydration, carbonization, swelling, and oxidization, in the concentrated H_2SO_4.[33] In terms of TEM observation, the crosslinking agent had less impact on the morphology of OMC, and this agreed well with the XRD analysis.

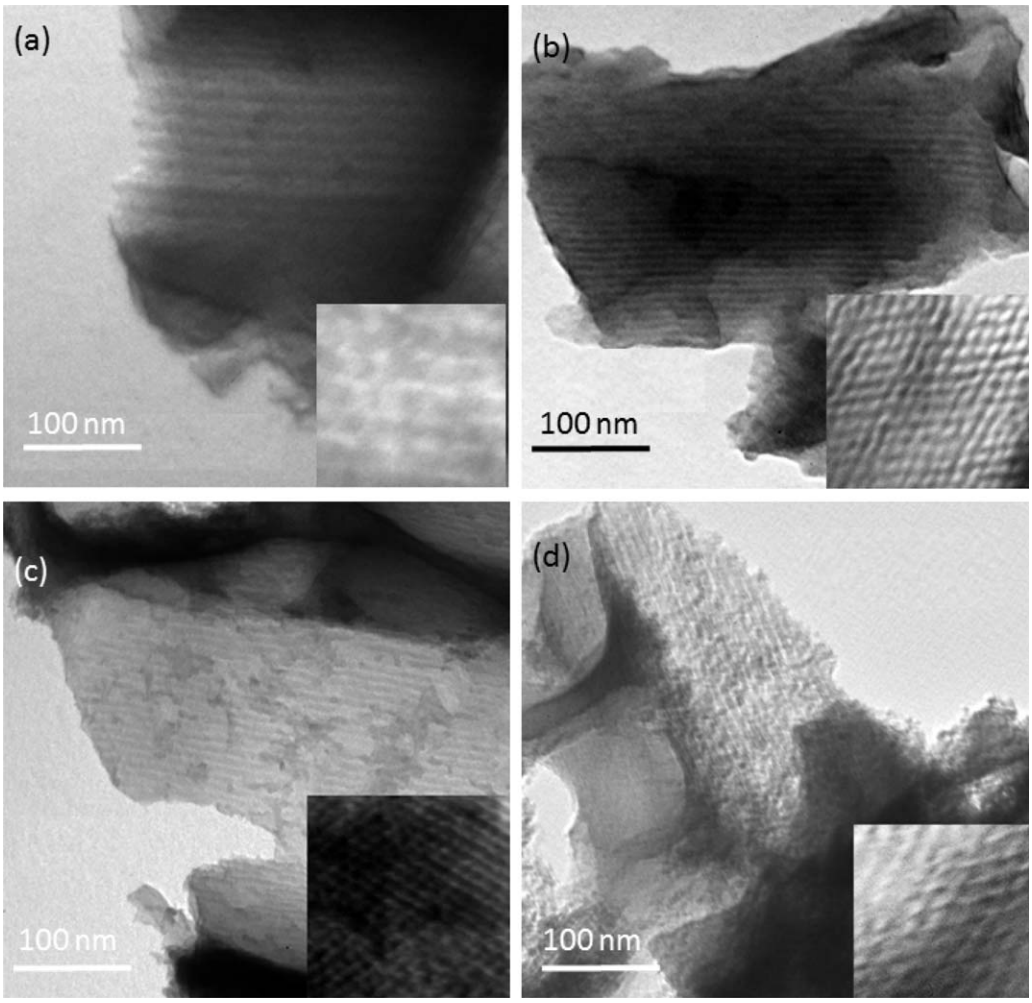

Figure 9. TEM images of the modified OMCs: (a) OMC-1, (b) OMC-2, (c) OMC-3, and (d) OMC-4.

Table II. SSAs of the SBA-15 and OMCs

Sample	SSA (m^2/g)	Sample	SSA (m^2/g)	Sample	SSA (m^2/g)
SBA-15-1	561	OMC-21	474	OMC-1	379
		OMC-31	422	OMC-2	443
SBA-15-2	597	OMC-22	518	OMC-3	516
		OMC-32	427	OMC-4	482
SBA-15-3	534	OMC-23	528	GAC	580
		OMC-33	551		

SSAs of the SBA-15 and OMCs

SSAs of the silica template and OMCs were measured by an N_2 adsorption–desorption method. The SSAs of the SBA-15 and corresponding OMCs are displayed in Table II. These results were similar to those of previous reports.[14,35] The results show that the change in the reaction conditions directly affected the SSA of SBA-15, and this further impacted the SSA of OMC. We concluded that the template with the higher SSA resulted in an OMC with a higher SSA; however, the trend in actual data did not match these assumptions. The results may have been caused by the shrinkage and collapse during the fabrication process. Compared with silica templates, the SSAs of OMCs decreased in most cases and increased in OMC-33; this showed that the template was not the only factor that determined the SSA of OMC.[37] We also noticed that the final SSA of OMC was affected by the amount of SBA-15.[31,32] Because the channel walls were formed by the carbon source (monomer) and the mesopores were formed by the etching of the SBA-15, when the pores were partially filled, the resulting OMC might have generated broken channel walls and became less ordered. On the contrary, completely filled mesopores could have resulted in well-organized channel walls.

All of the modified OMCs had a smaller SSA compared with OMC-22, but the difference was not significant, except that of OMC-1. This may have been caused by the shrinkage of the pore structure because of the strong oxidation reaction between the carbon precursor and H_2SO_4. The crosslinking agent bridged the molecular chain (as shown in Figure 1) and increased the molecular weight of the polyacrylamide (PAM) to increase its resistance to H_2SO_4, and the melamine could generate some nitrogen gas during heating to offset part of the shrinkage. Therefore, the decrease in SSA was insignificant, even though H_2SO_4 was also added in OMC-3 and OMC-4. Therefore, the modification of the carbon precursor had no significant influence on the SSA of the final OMC.

Nitrogen Sorption Isotherms and Pore Size Distribution

Further analysis of the N_2 sorption isotherms and pore size distribution were conducted for OMC-22 and the modified OMCs. As shown in Figure 10(a), all of the nitrogen adsorption isotherm curves showed a representative type IV curve with H1 hysteresis; this suggested the formation of cylindrical pore channels.[2–8] The gradual increase in the adsorption volume of the sorption isotherm curve located at low relative pressure ($P/P_0 < 0.3$, where P and P_0 are the equilibrium and saturation pressure of adsorbates) might indicate the existence of abundant micropores less than 2 nm in the materials. The relatively steep nitrogen uptake step in all of the isotherm curves proved the presence of uniform mesopores.[4,6,7] The pore size distribution in Figure 10(b) demonstrated that OMC-22, OMC-1, and OMC-2 had a narrow pore size distribution of around 6–8 nm. OMC-4 had as slightly larger pore size in the mesopore range, whereas OMC-3 displayed a wide pore size distribution centered around 50 nm. These results were reasonably consistent with the TEM characterization, except for that of OMC-3; this might have been due to the combined effect of H_2SO_4 and crosslinker.

FTIR and Raman Spectra Analysis

FTIR and Raman spectroscopy were used to detect possible functional groups and changes in the chemical bonds, which could be attributed to the modifications of the carbon precursor. As shown in Figures 11 and 12, modified OMCs had similar chemical structures to OMC-22. Specifically, in Figure 11, (1) the weak small bands ranging from 3500 to 3950 cm^{-1} may have resulted from the —OH stretching vibrations[3,13,21] because of the adsorption of moisture, (2) the strong peaks centered around 1700 cm^{-1} could be ascribed to C=O[14,26] resulting from PAM, and (3) the bands near 860 cm^{-1} and those between 1460–1560 cm^{-1} may have been caused by the stretching vibrations of C—H[21] and C—N,[38] respectively. Stronger peaks were observed in Figure 11(b–d) between 2285 and 2400 cm^{-1}; these peaks were assigned to C—O,[21] or some trapped N_2[39] because of the pyrolysis of the added chemicals. As shown in Figure 11(b), a sharp peak at

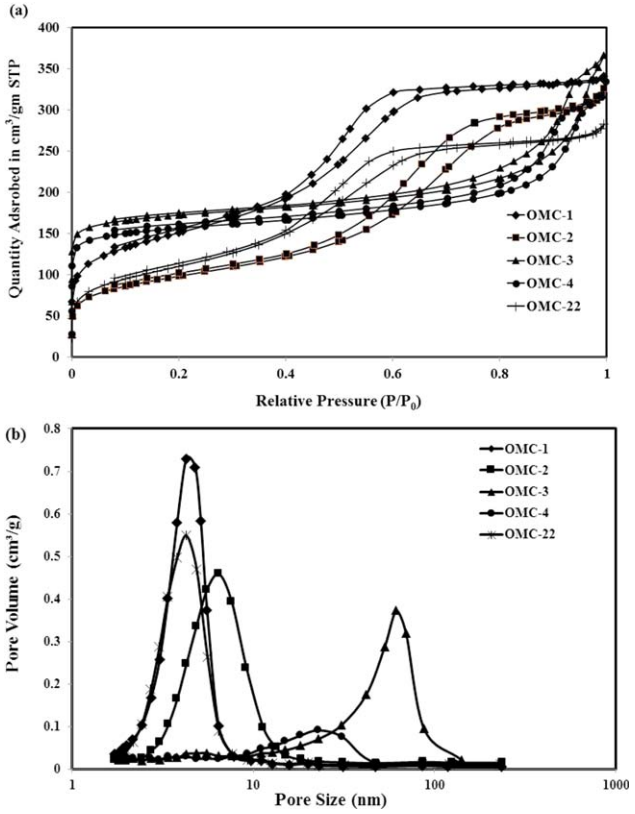

Figure 10. (a) N_2 sorption isotherms and (b) corresponding pore size distributions of the modified OMCs and OMC-22. [Color figure can be viewed in the online issue, which is available at wileyonlinelibrary.com.]

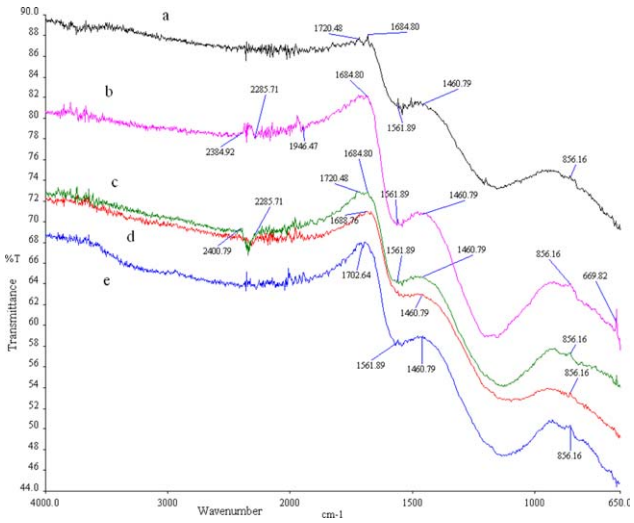

Figure 11. FTIR spectra of (a) OMC-1, (b) OMC-4, (c) OMC-2, (d) OMC-3, and (e) OMC-22. [Color figure can be viewed in the online issue, which is available at wileyonlinelibrary.com.]

670 cm^{-1} was observed; this may have been caused by C—OH stretching vibrations,[40] which resulted from the reaction between H_2SO_4 and melamine. At the same time, the peak around 1685 cm^{-1} was steeper than the other peaks; this was attributed to the strong stretching vibrations of C═N[41] introduced by melamine.

In Figure 12, the strong D band located around 1300 cm^{-1} was related to the disordered graphite structure and defects and could be attributed to C—O stretching.[42,43] We found that precursor modification increased the defect sites in carbon materials, and this made posttreatment easier. The G band around 1600 cm^{-1} was not very significant, but relatively small peaks could be detected as the stretching of C═O vibrations;[42] this was consistent with FTIR analysis. These peaks around 2300 cm^{-1} could be attributed to graphitic lattice vibration modes[43] and may have resulted from the C—N vibrations.[44] These peaks around 300 cm^{-1} were assigned to the —OH and —H bond vibrations,[45] but they may have resulted

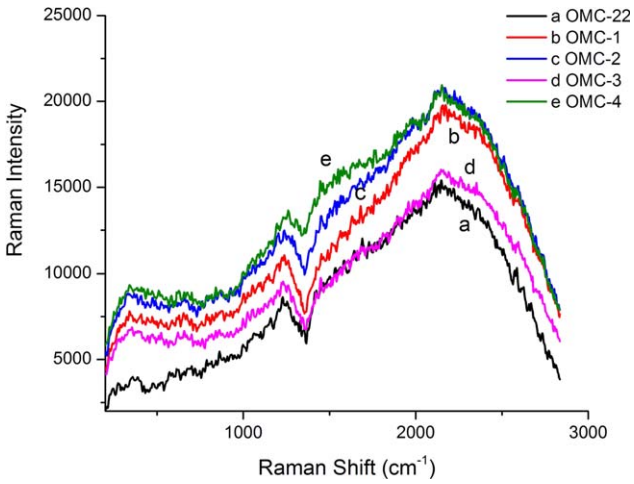

Figure 12. Raman spectra of the OMC-22 and modified OMCs. [Color figure can be viewed in the online issue, which is available at wileyonlinelibrary.com.]

Table III. Elemental Compositions of the OMC-22 and Modified OMCs

Sample	C	N	H	O
OMC-22	75.29	12.44	1.24	10.92
OMC-1	68.80	11.91	1.71	13.71
OMC-2	76.84	12.81	1.49	8.57
OMC-3	71.08	11.98	1.66	13.97
OMC-4	71.47	13.51	1.41	10.05

from the adsorption of moisture. These results proved that addition of H_2SO_4 and melamine affected the pore structure of the final OMC to a certain degree; however, the influence of the crosslinking agent was not significant because it only changed the PAM structure instead of its functional group.

Element Analysis

Table III shows the slight increases in C, N, and H in OMC-2 compared with OMC-22; this resulted from the crosslinking effect. Both N and H elements favored the adsorption capacity. OMC-3 and OMC-1 had the same trends of elemental increase (H, O) and decrease (C, N), this trend was related to H_2SO_4; however, because of the crosslinking reaction in OMC-3, it had less of a decrease. The oxygen was induced by the oxidation of polymer by H_2SO_4; this could contribute to the adsorption of resorcinol. In OMC-4, N increased slightly compared to that of the other OMCs, and this was caused by the addition of melamine. The existence of N, H, and O elements enhanced the interactions between OMC and resorcinol and, hence, improved the adsorption capacity through weak forces, such as hydrogen bonds.[14,21,24]

Adsorption Capacity Evaluation

The adsorption capacities for resorcinol removal were compared between OMCs and commercial granular activated carbon (GAC; Norit). GAC is a chemically activated granular carbon produced by a phosphoric acid activation process. All of the data were obtained within 2 weeks after the samples were fabricated. As shown in Figure 13, the OMCs had a higher adsorption capacity

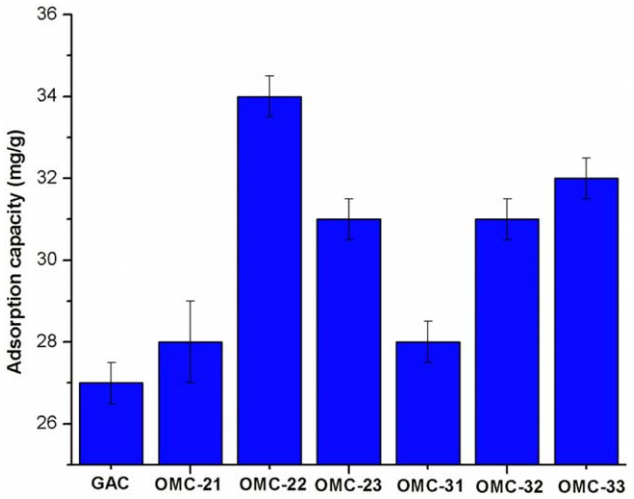

Figure 13. Adsorption capacities of resorcinol on the GAC and OMCs obtained at an adsorption temperature of 25 °C with an adsorbent dose of 0.1 g/L and an adsorption time of 24 h. [Color figure can be viewed in the online issue, which is available at wileyonlinelibrary.com.]

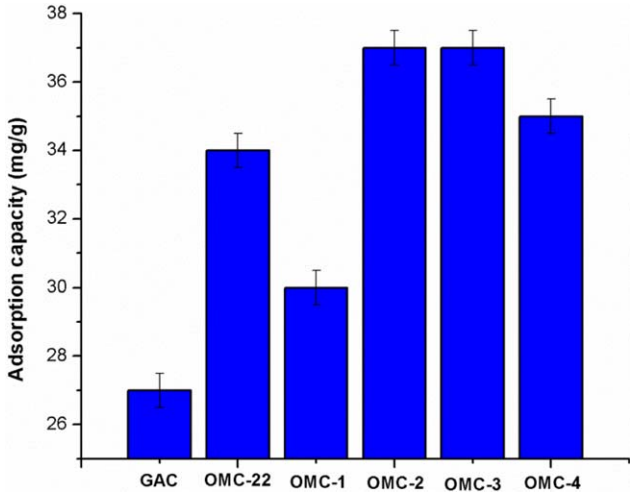

Figure 14. Adsorption capacities of resorcinol on GAC and modified OMCs obtained at an adsorption temperature of 25 °C with an adsorbent dose of 0.1 g/L and an adsorption time of 24 h. [Color figure can be viewed in the online issue, which is available at wileyonlinelibrary.com.]

than GAC (27 mg/g); it ranged from 28 to 34 mg/g. Among these OMCs, OMC-22 had the highest adsorption capacity; it was about 26% higher than that of GAC. The results did not show a significant influence of the SBA-15 amount (either 2 or 3 g) on the adsorption capacity in the investigated cases, except for OMC-22 and OMC-23; however, we observed that the ratio between the template and monomer had significant effects on the polymerization speed and product. It is also believed that the ratio affected the purity of OMC and, thereby, impacted the adsorption capacity. In this study, the addition of 2 g of SBA-15 to the 10 g of the AM solution might have already been saturated, as some white powder was observed after *in situ* polymerization. The results show that the OMCs replicated from SBA-15-2 had higher adsorption capacities than the ones replicated from SBA-15-1 and SBA-15-3, whereas the ones made from SBA-15-1 had the lowest adsorption capacity. It seemed that SBA-15-2 was a good template for the fabricated OMC, and 2 g was appropriate for 10 g of AM.

Figure 14 compares the adsorption capacity of the OMC-22 and modified OMCs. OMC-2 and OMC-3 with crosslinking agent showed the highest adsorption capacity (37 mg/g); this was 37% higher than that of GAC and 8.8% higher than that of the original OMC-22. The adsorption capacity of active carbon predicted by Kumar *et al.*[46] was less than 30 mg/g at a low concentration of resorcinol; this was lower than the OMC studied here. Liao *et al.*[47] reported that the adsorption of resorcinol by multiwalled carbon nanotubes at an initial concentration of 100 mg/L was about 31 mg/g; this was lower than those of OMC-22, OMC-2, and OMC-3. The adsorption percentage of OMC investigated in this study was about 75% at a very low material loading of 10 mg for a low concentration (5 mg/L) resorcinol solution; this was higher than that of activated carbon made from coffee grounds.[48] The OMCs also performed better than $ZnCl_2$-activated coir pith carbon.[49] These results suggest the favorable influence of the crosslinking agent in improving the adsorption capacity of the studied OMC. As discussed previously, the main characteristics (morphology, pore size, and SSA) of these modified OMCs were similar except for those of OMC-3; thus, the improvement of adsorption the capacity mainly resulted from the different chemical compositions, namely, those of the heteroatoms (O and N). Also, we noticed that when the crosslinking agent was added, the OMC yield was improved from 2 to 3 g, with an improvement of 50%. We believe that the crosslinking agent not only induced the nitrogen element to favor the adsorption performance[14,21,25] but also changed the PAM structure from linear two dimensional to three dimensional (partially shown in Figure 1) and increased the molecular weight and, thereby, reduced the pyrolysis of PAM. The adsorption capacity of OMC-1 was slightly lower than that of OMC-22; this meant that the single effect of H_2SO_4 was not good and may have even damaged the mesoporous structure [as shown in Figure 5(b)] and reduced SSA. However, because of the relatively mild dehydration carbonization process, more carbon material was fixed, and a higher yield (ca. 40%) of OMC was observed. The addition of melamine (OMC-4) caused no significant improvement in the adsorption, although melamine was applied as a nitrogen source. However, because of its low solubility and instability, the presence of nitrogen in the finally prepared OMC was very limited. We believe that better performance could be achieved by optimization of the melamine dose and by changing its introducing method. We observed that the adsorption capacities of the OMCs were partially correlated to their SSAs; this means that higher SSA induced a higher adsorption capacity.

If one recalls the SSAs of the OMCs and GAC, one can infer that the ordered mesopores favored the adsorption capacity over the SSA. Although no significant changes were observed, as depicted in Figure 9 through carbon precursor modification, the improved adsorption capacity may have been due to the increase in adsorption sites, such as C—O and C—N bonds; this could directly or indirectly drive the interaction between OMC and resorcinol through hydrogen bonds.[14,21,24] It is worth noting that OMCs derived from different carbon precursors can affect the adsorption;[14] therefore, the emphasis of this study was to evaluate the modification of carbon precursors, such as AM, especially through the addition of the crosslinking agent. Extra posttreatment could be applied in the previously modified OMC to further improve its adsorption capacity. The modification method proposed here could easily be extended to other polymer systems and would, thereby, promote the design of multifunctional adsorbents.

CONCLUSIONS

This study demonstrated that AM could be used as a carbon precursor to fabricate OMC. Several approaches were used to modify the OMC to improve its adsorption capacity. Generally, the addition of crosslinking agent and melamine showed good potential for adsorption capacity improvement, and the crosslinking agent could improve the carbon yield. The use of concentrated H_2SO_4 did not show direct improvement in the adsorption capacity and could damage the mesostructure,

although a higher yield (ca. 40%) of OMC was obtained. The characterization of the pore structure and the evaluation of the adsorption capacity revealed that the modification of the precursor with crosslinking agent could not only just preserve the ordered mesoporous structure but could also improve the adsorption capacity through the introduction of the heteroatom (N) from the carbon precursor. In light of this research, it should be possible to fabricate superior adsorbents suitable for the removal of different pollutants through the incorporation of diverse polymers as carbon precursors.

ACKNOWLEDGMENTS

This work was supported by the Louisiana Board of Regents through the Board of Regents Support Fund (2010–2015)/Louisiana Space Consortium and by the National Aeronautics and Space Administration through award NNX10AI40H.

REFERENCES

1. Zhang, Y. H.; Wang, A. Q.; Zhang, T. *Chem. Commun.* **2010**, *46*, 862.
2. Su, F. B.; Zeng, J. H.; Bao, X. Y.; Yu, Y. S.; Lee, J. Y.; Zhao, X. S. *Chem. Mater.* **2005**, *17*, 3960.
3. Wang, Y. G.; Li, H. Q.; Xia, Y. Y. *Adv. Mater.* **2006**, *18*, 2619.
4. Chi, Y.; Geng, W.; Zhao, L.; Yan, X.; Yuan, Q.; Li, N.; Li, X. T. *J. Colloid Interface Sci.* **2012**, *369*, 366.
5. Liu, Y.; Zeng, Z.; Zeng, G.; Tang, L.; Pang, Y.; Li, Z.; Liu, C.; Lei, X. X.; Wu, M. S.; Ren, P. Y.; Liu, Z. F.; Chen, M.; Xie, G. X. *Bioresour. Technol.* **2012**, *115*, 21.
6. Ryoo, R.; Joo, S. H.; Kruk, M.; Jaroniec, M. *Adv. Mater.* **2001**, *13*, 677.
7. Yu, C.; Fan, J.; Tian, B.; Zhao, D. Y.; Stucky, G. D. *Adv. Mater.* **2002**, *14*, 1742.
8. Liang, C.; Li, Z.; Dai, S. *Angew. Chem. Int. Ed.* **2008**, *47*, 3696.
9. Zhang, F.; Meng, Y.; Gu, D.; Yan, Y.; Yu, C.; Tu, B.; Zhao, D. *J. Am. Chem. Soc.* **2005**, *127*, 13508.
10. Liu, D.; Lei, J. H.; Guo, L. P.; Deng, K. *J. Carbon* **2011**, *49*, 2113.
11. Liu, D.; Lei, J. H.; Guo, L. P.; Qu, D.; Li, Y.; Su, B. L. *Carbon* **2012**, *50*, 476.
12. Ghimbeu, C. M.; Vidal, L.; Delmotte, L.; Meins, J. L.; Guterl, C. *Green Chem.* **2014**, *16*, 3079.
13. Ryoo, R.; Joo, S. H.; Jun, S. *J. Phys. Chem. B* **1999**, *103*, 7743.
14. Guo, R.; Guo, J.; Yu, F.; Gang, D. D. *Microporous Mesoporous Mater.* **2013**, *175*, 141.
15. Yang, C. M.; Weidenthaler, C.; Spliethoff, B.; Mayanna, M.; Schuth, F. *Chem. Mater.* **2005**, *17*, 355.
16. Kruk, M.; Dufour, B.; Celer, E. B.; Kowalewski, T.; Jaroniec, M.; Matyjaszewski, K. *J. Phys. Chem. B* **2005**, *109*, 9216.
17. Liang, C.; Hong, K.; Guiochon, G. A.; Mays, J. W.; Dai, S. *Angew. Chem. Int. Ed.* **2004**, *43*, 5785.
18. Anirudhan, T. S.; Sreekumari, S. S.; Bringle, C. D. *Adsorption* **2009**, *15*, 439.
19. Hameed, B. H.; Rahman, A. A. *J. Hazard. Mater.* **2008**, *160*, 576.
20. Nollet, L. M. L.; Gelder, L. S. P. Handbook of Water Analysis, 2nd ed.; CRC: Boca Raton, FL, **2007**.
21. Cansado, I. P. P.; Mourao, P. A. M.; Falcao, A. I.; Ribeiro Carrott, M. M. L.; Carrott, P. J. M. *Fuel Process. Technol.* **2012**, *103*, 64.
22. Kallel, M.; Belaid, C.; Mechichi, T.; Ksibi, M.; Elleuch, B. *Chem. Eng. J.* **2009**, *150*, 391.
23. Melo-Guimarães, A.; Torner-Morales, F. J.; Duran-Alvarez, J. C.; Jimenez-Cisneros, B. E. *Water Sci. Technol.* **2013**, *67*, 877.
24. Li, Q.; Yu, H.; Song, J.; Pan, X.; Liu, J.; Wang, Y.; Tang, L. *Appl. Surf. Sci.* **2014**, *290*, 260.
25. Anbia, M.; Ghaffari, A. *Appl. Surf. Sci.* **2009**, *255*, 9487.
26. He, J.; Ma, K.; Jin, J.; Dong, Z.; Wang, J.; Li, R. *Micropor. Mesopor. Mater.* **2009**, *121*, 173.
27. Li, H.; Xi, H.; Zhu, S.; Wen, Z.; Wang, R. *Micropor. Mesopor. Mater.* **2006**, *96*, 357.
28. Bazuła, P. A.; Lu, A. H.; Nitz, J. J.; Schuth, F. *Micropor. Mesopor. Mater.* **2008**, *108*, 266.
29. Karagöz, S.; Tay, T.; Ucar, S.; Erdem, M. *Bioresour. Technol.* **2008**, *99*, 6214.
30. Zhao, D.; Feng, J.; Huo, Q.; Melosh, N.; Fredickson, G. H.; Chmelka, B. F.; Stucky, G. D. *Science* **1998**, *279*, 548.
31. Vinu, A.; Srinivasu, P.; Takahashi, M.; Mori, T.; Balasubramanian, V. V.; Ariga, K. *Micropor. Mesopor. Mater.* **2007**, *100*, 20.
32. Ignat, M.; Oers, C. J.; Vernimmen, J.; Mertens, M.; Potgieter-Vermaak, S.; Meynen, V.; Popovici, E.; Cool, P. *Carbon* **2010**, *48*, 1609.
33. Jang, M.; Kamens, R. *Environ. Sci. Technol.* **2001**, *35*, 4758.
34. Hiremath, J.; Vishalakshi, B. *Pharma Chem.* **2012**, *4*, 946.
35. Björk, E. M.; Söderlind, F.; Odén, M. *J. Colloid Interface Sci.* **2014**, *413*, 1.
36. Lee, J.; Joo, S. H.; Ryoo, R. *J. Am. Chem. Soc.* **2002**, *124*, 1156.
37. Yuan, X.; Xing, W.; Zhuo, S.; Si, W.; Gao, X.; Han, Z.; Yan, Z. F. *J. Colloid Interface Sci.* **2008**, *322*, 558.
38. Krishnakumar, V.; Xavier, R. *J. Spectrochim. Acta A* **2004**, *60*, 709.
39. Wakabayashi, F.; Kondo, J.; Wada, A.; Domen, K.; Hirose, C. *J. Phys. Chem.* **1993**, *97*, 10761.
40. Schwanninger, M.; Rodrigues, J. C.; Pereira, H.; Hinterstoisser, B. *Vib. Spectrosc.* **2004**, *36*, 23.
41. Socrates, G. Infrared and Raman Characteristic Group Frequencies: Tables and Charts, 3rd ed.; Wiley: Hoboken, NJ, **2004**.
42. Beyere, L.; Yarasi, S.; Loppnow, G. R. *J. Raman Spectrosc.* **2003**, *34*, 743.

43. Sadezky, A.; Muckenhuber, H.; Grothe, H.; Niessner, R.; Poschl, U. *Carbon* **2005**, *43*, 1731.

44. Ferrari, A. C.; Rodil, S. E.; Robertson, J. *Diamond Relat. Mater.* **2003**, *12*, 905.

45. Jehlička, J.; Edwards, H. G. M.; Culka, A. *Philos. Trans. R. Soc. London Ser A* **2010**, *368*, 3109.

46. Kumar, A.; Kumar, S.; Kumar, S. *Carbon* **2003**, *41*, 3015.

47. Liao, Q.; Sun, J.; Gao, L. *Colloids Surf. A* **2008**, *312*, 160.

48. Namane, A.; Mekarzia, A.; Benrachedi, K.; Belhaneche-Bensemra, N.; Hellal, A. *J. Hazard. Mater.* **2005**, *119*, 189.

49. Namasivayam, C.; Sangeetha, D. *J. Hazard. Mater.* **2006**, *135*, 449.